

Development and Persistence of ‘Static’ or ‘Dead’ Zones in Flows

Problem Presenter

John Abbott
Corning, Inc.

Problem Participants

Richard Braun, University of Delaware
Chris Breward, Oxford University
L. Pamela Cook, University of Delaware
Mike Cromer, University of Delaware
David A. Edwards, University of Delaware
Joseph Hibdon, Northwestern University
Colin Please, University of Southampton
Michele Taroni, Oxford University
Shangyou Zhang, University of Delaware
and others...

Twenty-Fifth Annual Workshop on Mathematical Problems in Industry
June 15–19, 2009
University of Delaware

Section 1: Introduction

Certain ceramic products are formed through extrusion processes, where a slurry is forced through small openings to form such products as filters. A typical device is shown in Figure 1.1. At the top is a large tank. The slurry is forced through the tank into an extrusion chamber, and then out through slots to form the finished product.

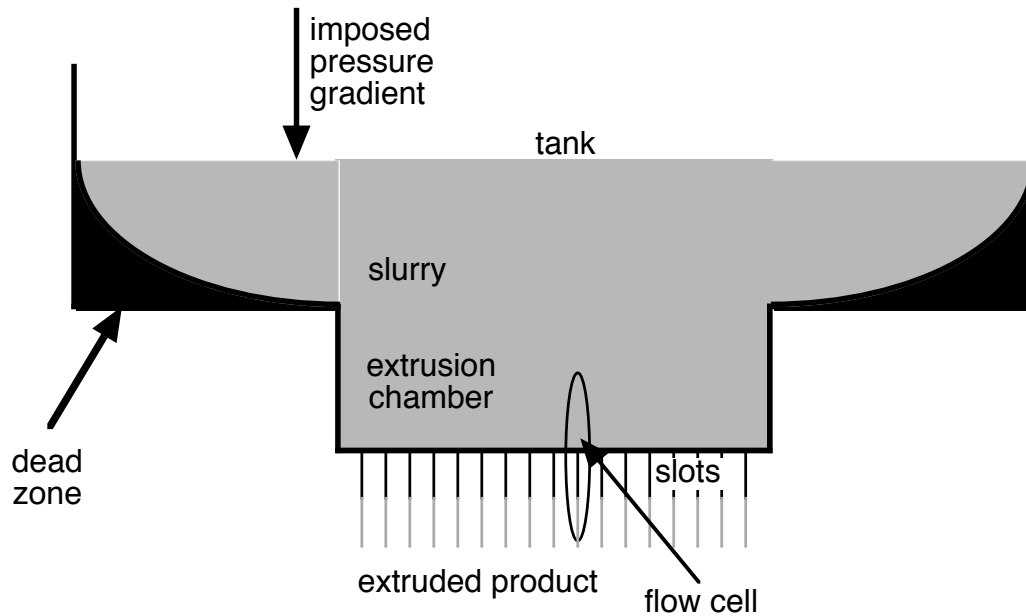


Figure 1.1. Schematic of extrusion device. The flow cell of interest is magnified in Figure 1.2.

The slurry may be thought of as a mixture of clay (or other polymers), water, and other binders. There are many ways to model this mixture, some of which will be discussed in this report. For instance, the slurry can be modeled as a non-Newtonian fluid (see section 3), a two-phase flow with liquid and solids, or a viscoelastic fluid. One can also model the mixture as an elongated particle suspension in water, where changes in the orientation of the particles could affect the flow.

After the extrusion process is complete, one finds that ‘dead zones’ of dry paste accumulate in two areas. Most prominently, they occur at the lower corners of the tank (see Figures 1.1 and 1.2). They also occur on the floor of the extrusion chamber near the slots, both near and away from the walls. Since we will consider wall effects in the tank, for the extrusion chamber we consider only *flow cells* sufficiently far away from the walls. Then we may exploit the periodic nature of the device and consider only a single flow cell, as illustrated in Figure 1.3.

The aim of this project is to determine the formation mechanisms of these dead zones, and see how they affect the overall flow.

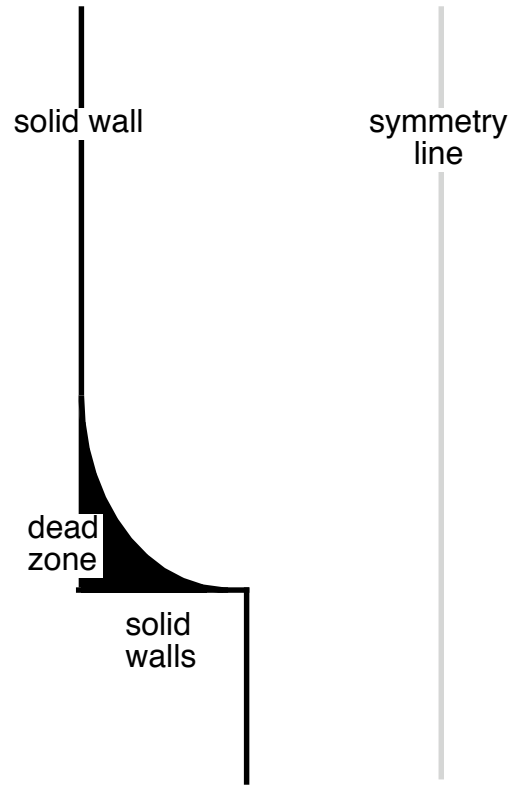


Figure 1.2. Schematic of half of the tank.

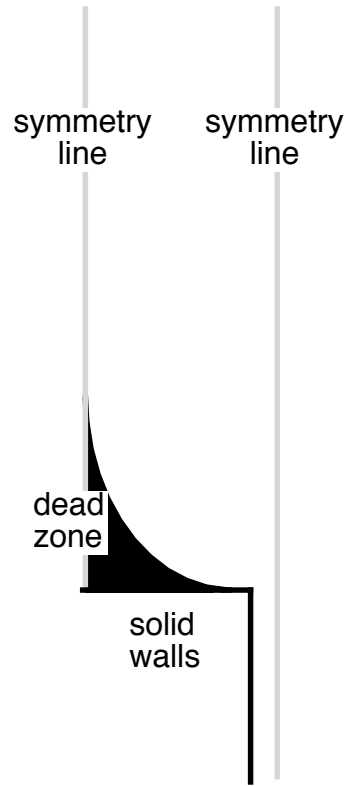


Figure 1.3. Flow cell in extrusion chamber.

Section 2: Mathematical Model

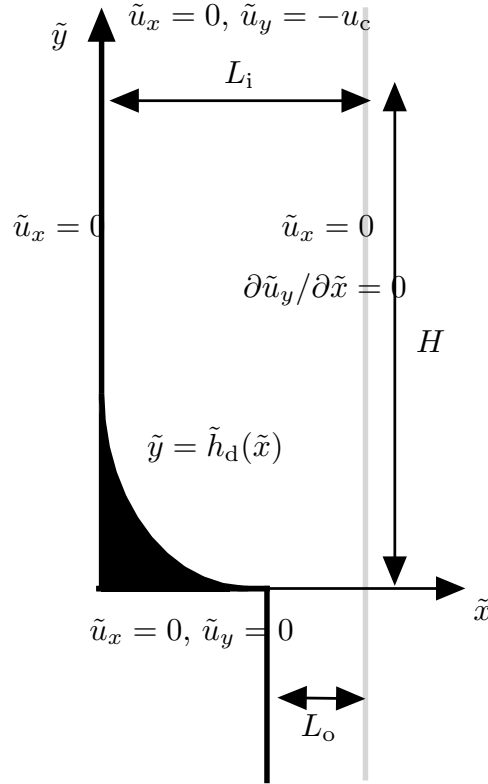


Figure 2.1. Geometry under consideration.

We denote the flow velocity as $(\tilde{u}_x, \tilde{u}_y)$. We see from the similarities between Figure 1.2 and Figure 1.3 that we may use the same geometry for both regions; only the boundary condition on \tilde{u}_y at the left boundary will change. We assume a two-dimensional geometry, with the origin in (\tilde{x}, \tilde{y}) space at the intersection of the left boundary and the floor (see Figure 2.1). The region has width L_i (where the subscript “i” refers to “input”) and the part of the passage to the next region has width L_o (where the subscript “o” refers to “output”). The region has height H above the floor. The dead zone is described as the region under the curve $\tilde{y} = \tilde{h}_d(\tilde{x})$.

Because of the symmetries, we obtain

$$\tilde{u}_x(0, \tilde{y}) = \tilde{u}_x(L_i, \tilde{y}) = \tilde{u}_y(0, \tilde{y}) = 0, \quad \frac{\partial \tilde{u}_y}{\partial \tilde{x}}(L_i, \tilde{y}) = 0. \quad (2.1)$$

In addition, because of the floor and channel conditions, we have the following:

$$\tilde{u}_x(\tilde{x}, 0) = \tilde{u}_y(\tilde{x}, 0) = 0; \quad \tilde{u}_x(L_i - L_o, \tilde{y}) = \tilde{u}_y(L_i - L_o, \tilde{y}) = 0, \quad \tilde{y} < 0. \quad (2.2)$$

At the top of the cell, a constant vertical flow $-u_c$ is imposed, so we have that

$$\tilde{u}_x(\tilde{x}, H) = 0, \quad \tilde{u}_y(\tilde{x}, H) = -u_c. \quad (2.3)$$

In this geometry, conservation of mass becomes

$$\frac{\partial \tilde{u}_x}{\partial \tilde{x}} + \frac{\partial \tilde{u}_y}{\partial \tilde{y}} = 0. \quad (2.4)$$

At first glance, we may wish to exploit the fact that $L_i \ll H$ to create a lubrication-type problem. However, in the flow cell, $\tilde{x} = 0$ and $\tilde{x} = L$ are lines of symmetry, so the solution in the region away from $\tilde{y} = 0$ is just plug flow with $\tilde{u}_x = 0$, $\tilde{u}_y = -u_c$. Similarly, it will be shown that in the tank, the flow far from $\tilde{y} = 0$ will also be plug flow.

Therefore, instead we scale both \tilde{x} and \tilde{y} with L_i :

$$x = \frac{\tilde{x}}{L_i}, \quad y = \frac{\tilde{y}}{L_i}, \quad u_x(x, y) = \frac{\tilde{u}_x(\tilde{x}, \tilde{y})}{u_c}, \quad u_y(x, y) = \frac{\tilde{u}_y(\tilde{x}, \tilde{y})}{u_c}. \quad (2.5)$$

Substituting these results into (2.1)–(2.3), we obtain the following conditions on u_x :

$$u_x(0, y) = u_x(1, y) = u_x(x, 0) = u(x, \infty) = 0, \quad u_x(1 - \ell, y) = 0, \quad y < 0; \quad \ell = \frac{L_o}{L_i}, \quad (2.6)$$

where we have exploited the fact that $H \gg L_i$ to model the top of the chamber as $y \rightarrow \infty$. In other words, we are considering y to be an “inner variable.”

In addition, we obtain the following conditions on u_y :

$$u_y(x, \infty) = -1, \quad \frac{\partial u_y}{\partial x}(1, y) = u_y(x, 0) = 0; \quad u_y(1 - \ell, y) = 0, \quad y < 0, \quad (2.7a)$$

$$u_y(0, y) = 0. \quad (2.7b)$$

Lastly, conservation of mass remains balanced:

$$\frac{\partial u_x}{\partial x} + \frac{\partial u_y}{\partial y} = 0. \quad (2.8)$$

With these scalings, the Reynolds number is defined by

$$\text{Re} = \frac{\rho u_c L_i}{\eta_c}, \quad (2.9)$$

where η_c is a characteristic viscosity of the fluid and ρ is the density. Since the Reynolds number is small (see Appendix), we may neglect the inertial terms in the Navier-Stokes equations. Since we may wish to treat the fluid as non-Newtonian, we write conservation of linear momentum in terms of the stress tensor \tilde{T} , which has elements $\tilde{\tau}$:

$$-\frac{\partial \tilde{p}}{\partial \tilde{x}} + \frac{\partial \tilde{\tau}_{xx}}{\partial \tilde{x}} + \frac{\partial \tilde{\tau}_{yx}}{\partial \tilde{y}} = 0, \quad (2.10a)$$

$$-\frac{\partial \tilde{p}}{\partial \tilde{y}} + \frac{\partial \tilde{\tau}_{xy}}{\partial \tilde{x}} + \frac{\partial \tilde{\tau}_{yy}}{\partial \tilde{y}} = 0, \quad (2.10b)$$

where \tilde{p} is the pressure.

If we denote the strain tensor by \tilde{E} , we know that for Newtonian fluids,

$$\tilde{T} = \eta_c \tilde{E}, \quad (2.11)$$

where η_c is the (constant) viscosity. (Here the strain tensor is defined without the coefficient 1/2.) This motivates the scalings

$$E(x, y) = \frac{L_i \tilde{E}(\tilde{x}, \tilde{y})}{u_c}, \quad T(x, y) = \frac{L_i \tilde{T}(\tilde{x}, \tilde{y})}{\eta_c u_c}, \quad p(x, y) = \frac{L_i \tilde{p}(\tilde{x}, \tilde{y})}{\eta_c u_c}. \quad (2.12)$$

Substituting (2.5) and (2.12) into (2.10) and (2.11), we retain the same balances:

$$-\frac{\partial p}{\partial x} + \frac{\partial \tau_{xx}}{\partial x} + \frac{\partial \tau_{yx}}{\partial y} = 0, \quad (2.13a)$$

$$-\frac{\partial p}{\partial y} + \frac{\partial \tau_{xy}}{\partial x} + \frac{\partial \tau_{yy}}{\partial y} = 0, \quad (2.13b)$$

$$T = E. \quad (2.14)$$

Section 3: Bingham Fluid

As a first approximation we treat the slurry as a Bingham fluid. (Unless otherwise noted, the analysis in this section is adapted from Smyrnaios and Tsamopoulos, 2001.)

In a Bingham fluid, we replace (2.11) by

$$\tilde{T} = \left(\eta_c + \frac{\tau_c}{|\tilde{E}|} \right) \tilde{E}, \quad |\tilde{T}| > \tau_c, \quad (3.1a)$$

$$\tilde{E} = O, \quad |\tilde{T}| < \tau_c, \quad (3.1b)$$

where τ_c is the *yield stress* and for any tensor A ,

$$|A| = \sqrt{\frac{A : A}{2}}. \quad (3.2)$$

Substituting (2.12) into (3.1), we obtain

$$\frac{\eta_c L_i}{u_c} T = \left(\eta_c + \frac{\tau_c u_c}{L_i |E|} \right) \frac{L_i}{u_c} E, \quad \frac{\eta_c L_i}{u_c} |T| > \tau_c$$

$$T = \left(1 + \frac{\text{Bn}}{|E|} \right) E, \quad |T| > \text{Bn}, \quad \text{Bn} = \frac{\tau_c L_i}{u_c \eta_c}. \quad (3.3a)$$

$$E = O, \quad |T| < \text{Bn}. \quad (3.3b)$$

Note that in this case the boundary $h_d(x)$ of the dead zone is a free no-slip boundary:

$$|T|(x, h_d(x)) = \text{Bn}, \quad u_x(x, h_d(x)) = u_y(x, h_d(x)) = 0. \quad (3.4)$$

For completeness, we write the modulus of the strain tensor in Cartesian coordinates:

$$|E| = \left\{ 2 \left[\left(\frac{\partial u_x}{\partial x} \right)^2 + \left(\frac{\partial u_y}{\partial y} \right)^2 \right] + \left(\frac{\partial u_x}{\partial y} + \frac{\partial u_y}{\partial x} \right)^2 \right\}^{1/2}. \quad (3.5)$$

We note that (3.3) has a jump discontinuity in T at $|E| = 0$. This may be reduced to a jump in the derivative with the following *biviscosity model* (Jay *et al.*, 2002):

$$\tilde{T} = \left(\eta_c + \frac{\tau_c}{|\tilde{E}|} \right) \tilde{E}, \quad |\tilde{E}| > E_c, \quad (3.6a)$$

$$\tilde{T} = \left(\eta_c + \frac{\tau_c}{|\tilde{E}_c|} \right) \tilde{E}, \quad |\tilde{E}| < E_c. \quad (3.6b)$$

To eliminate any jumps in the form of \tilde{T} (and hence the free-boundary problem), one may also consider the following exponential approximation (Papanastasiou, 1987):

$$\tilde{T} = \left[\eta_c + \frac{|\tilde{T}|(1 - e^{-\beta|\tilde{E}|})}{|\tilde{E}|} \right] \tilde{E}, \quad (3.7)$$

where $\beta > 0$ is a given constant.

Section 4: The Tank

The situation in the tank as been modelled and simulated numerically using the biviscosity model by Jay *et al.*, 2002, and using the exponential model by Adbali *et al.* (1992). In this section we attempt to describe their results numerically and analytically, as well as to extend them in special cases.

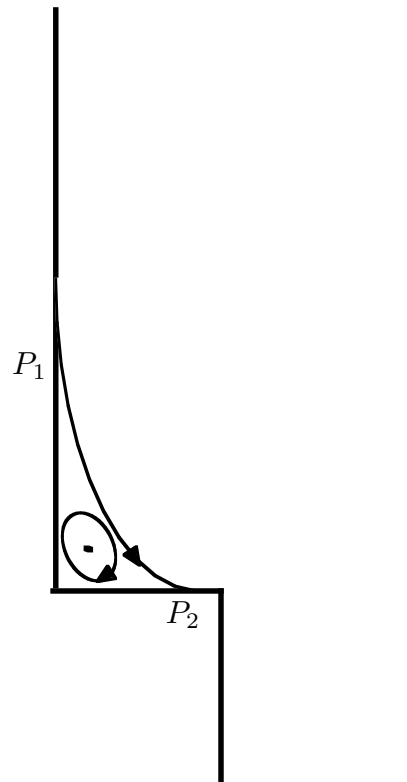


Figure 4.1. Schematic of separating streamline and recirculating Moffatt eddy for $Bn = 0$.

We begin by examining the limit where $Bn \rightarrow 0$, where the Bingham flow reduces to a perturbation of a Newtonian one. Since the Reynolds number is small, we have Stokes flow.

To visualize this flow, we performed a numerical simulation using a Fortran finite element code. It used continuous piecewise P_1 elements for the velocity and discontinuous piecewise P_0 elements for the pressure (with spurious modes filtered) with a Union-Jack grid (see Figure 4.2). We then constructed the velocity profiles (see Figures 4.2–4.4).

We note from the graphs that the velocity is quite small in the corners. For Stokes flow into a corner, we see that while the bulk of the flow squeezes through the nozzle, there will be a recirculation region near the corner. These *Moffatt eddies* (Moffatt, 1964) will

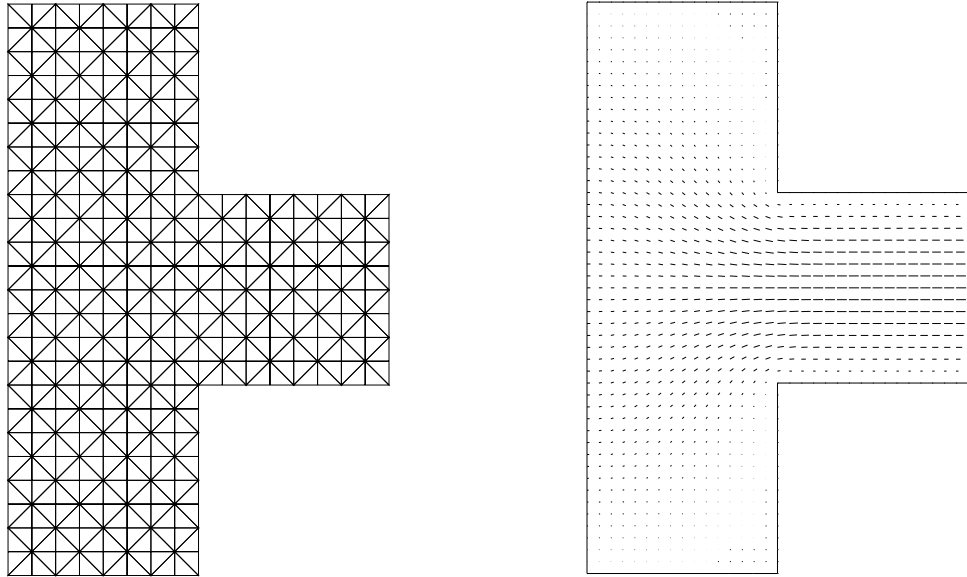


Figure 4.2. Left: grid used for simulation. Right: Velocity profile.

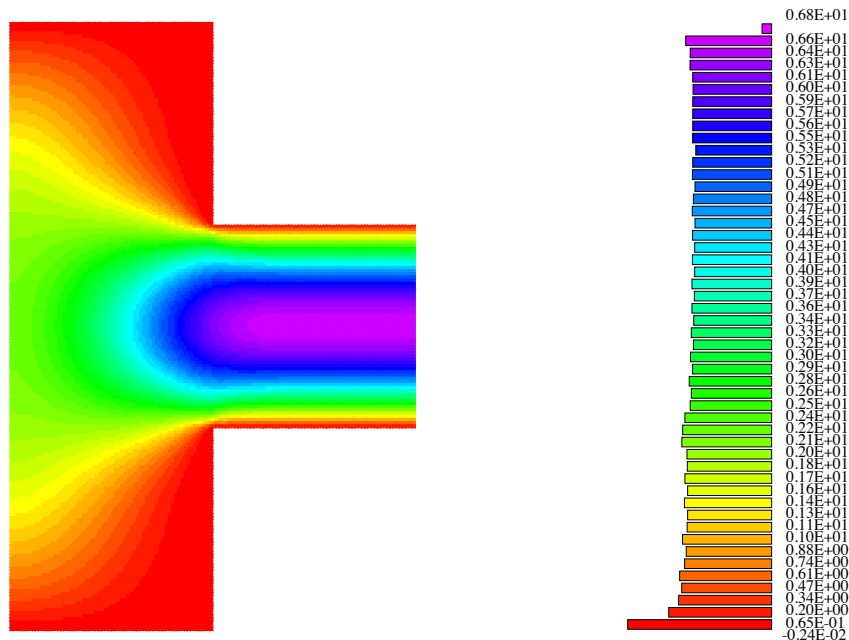


Figure 4.3. 2-D graph of velocity component in y -direction.

surround stationary points. However they can be quite small, which is why they may not have shown up in the simulation.

The proof of the eddy existence is as follows. Since we are now considering Stokes flow, we may use a stream function ψ to construct the flow. We expand around the corner using polar coordinates with $\theta = 0$ taken at the centerline of the corner (see Figure 4.4). Note then that the problem is symmetric about $\theta = 0$ and the wall corresponds to $\theta = \pi/4$.

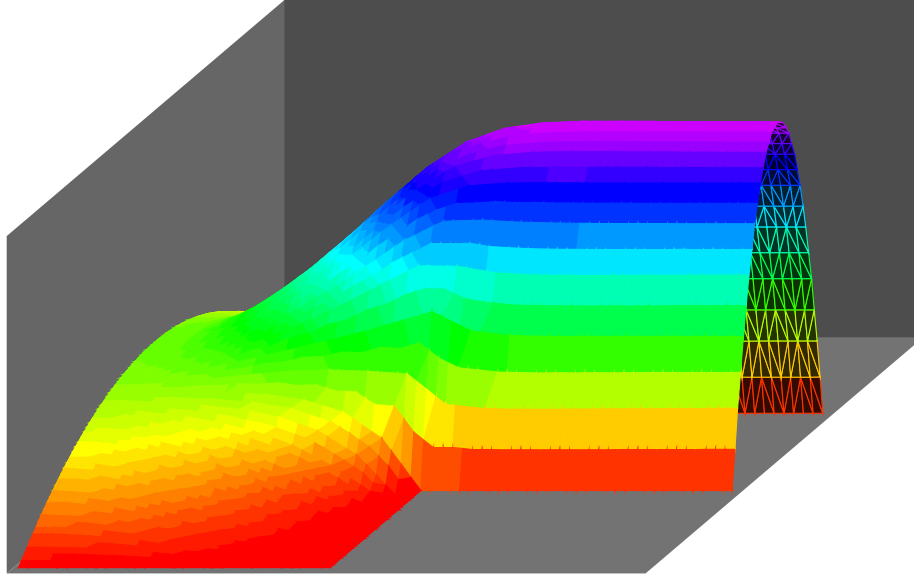


Figure 4.4. 3-D graph of velocity component in y -direction.

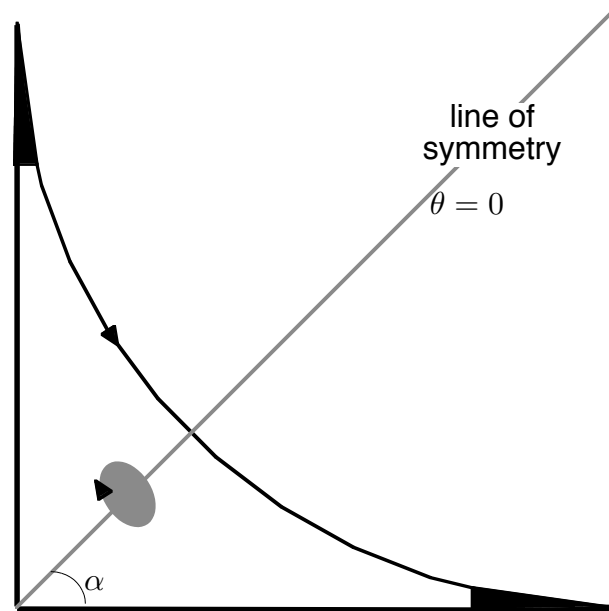


Figure 4.4. Tank flow for low Bingham number (magnified view near corner). The shaded regions are where the fluid is plastic, but moving. The dead zones are in black.

From Leal (1992), equations (4-94) and (4-124), we have

$$\nabla^4 \psi = 0, \quad u_r = \frac{1}{r} \frac{\partial \psi}{\partial \theta}, \quad u_\theta = -\frac{\partial \psi}{\partial r}, \quad (4.1)$$

and upon rearrangement of equation (4-119) it can be shown that a typical eigenfunction for the problem is given by

$$\psi = r^\lambda [A_c \cos \lambda \theta + A_s \sin \lambda \theta + B_c \cos(\lambda - 2)\theta + B_s \sin(\lambda - 2)\theta], \quad \lambda > 1, \quad \lambda \neq 2. \quad (4.2)$$

To obtain the leading-order behavior as $r \rightarrow 0$, we wish to consider the smallest possible λ .

From our geometry, we have that the problem is symmetric about $\theta = 0$ with

$$\begin{aligned} u_r(r, \theta) &= -u_r(r, -\theta) \\ \frac{\partial \psi}{\partial \theta}(r, -\theta) &= -\frac{\partial \psi}{\partial \theta}(r, \theta), \end{aligned} \quad (4.3)$$

which forces $A_s = B_s = 0$. Note that since the biharmonic equation is fourth order, we cannot use just the more standard boundary condition

$$u_r(r, 0) = 0,$$

since imposing this would result in an equation for A_s in terms of B_s . Due to this symmetry we may restrict our attention to the wedge $0 \leq \theta \leq \pi/4$.

From our geometry we also have that

$$\frac{\partial \psi}{\partial r}(r, \pi/4) = \frac{\partial \psi}{\partial \theta}(r, \pi/4) = 0. \quad (4.4)$$

For reasons that will become clear later, we set $\theta = \alpha$ at the wall, then substitute our exact value $\alpha = \pi/4$ at the end. Hence we have

$$\begin{aligned} \frac{\partial \psi}{\partial r}(r, \alpha) &= \lambda r^{\lambda-1} [A_c \cos(\lambda\alpha) + B_c \cos((\lambda-2)\alpha)] = 0 \\ \frac{\partial \psi}{\partial \theta}(r, \alpha) &= r^\lambda [-A_c \lambda \sin(\lambda\alpha) - B_c(\lambda-2) \sin((\lambda-2)\alpha)] = 0 \\ \cos((\lambda-2)\alpha) \lambda \sin(\lambda\alpha) [\cos(\lambda\alpha)]^{-1} &- (\lambda-2) \sin((\lambda-2)\alpha) = 0, \end{aligned}$$

where we have set the bracketed quantities in the first two equations equal to zero and set $B_c = 1$ without loss of generality. Continuing to simplify, we obtain

$$\begin{aligned} (\lambda-1) \cos((\lambda-2)\alpha) \sin(\lambda\alpha) &- (\lambda-1) \sin((\lambda-2)\alpha) \cos(\lambda\alpha) \\ &= -\cos((\lambda-2)\alpha) \sin(\lambda\alpha) - \sin((\lambda-2)\alpha) \cos(\lambda\alpha) \end{aligned}$$

$$(\lambda-1) \sin(2\alpha) = -\sin(2(\lambda-1)\alpha), \quad (4.5a)$$

$$\sin\left(\frac{\pi(\lambda-1)}{2}\right) = 1 - \lambda. \quad (4.5b)$$

Clearly there is no real solution of (4.5b) for $\lambda > 2$. For $1 < \lambda < 2$, we see that the left-hand side is positive while the right-hand side is negative. Hence there are no real solutions at all. Complex solutions lead to an infinite sequence of closed streamline eddies that accumulate at the corner (Leal, 1992, p. 158).

Near the eddy, we expect the flow to be in nearly solid body rotation, so we would have

$$u_\theta = 2Ar \quad \psi = -Ar^2 \quad u_r = 0, \quad (4.6)$$

where we have used the fact that we do not expect u_r to depend on θ . To examine the form of the stresses, we note from Bird *et al.* (1960), p. 89, that the components of the normalized Newtonian stress tensor in cylindrical coordinates are the following:

$$\tau_{rr} = 2 \frac{\partial u_r}{\partial r} = 2 \frac{\partial}{\partial r} \left(\frac{1}{r} \frac{\partial \psi}{\partial \theta} \right), \quad (4.7a)$$

$$\tau_{\theta\theta} = \frac{2}{r} \left(\frac{\partial u_\theta}{\partial \theta} + u_r \right) = \frac{2}{r} \left(-\frac{\partial^2 \psi}{\partial r \partial \theta} + \frac{1}{r} \frac{\partial \psi}{\partial \theta} \right), \quad (4.7b)$$

$$\tau_{r\theta} = r \frac{\partial}{\partial r} \left(\frac{u_\theta}{r} \right) + \frac{1}{r} \frac{\partial u_r}{\partial \theta} = r \frac{\partial}{\partial r} \left(-\frac{1}{r} \frac{\partial \psi}{\partial r} \right) + \frac{1}{r^2} \frac{\partial^2 \psi}{\partial \theta^2}, \quad (4.7c)$$

where we have flipped the sign convention for agreement. All of these terms vanish when the velocities are described by (4.6). Hence, we see that there is no stress in this region, and once we take $\text{Bn} \neq 0$, this is a place where a dead zone can form.

We attempted to see how the size of the dead zone varied for small Bn near these stationary points. Unfortunately, the analysis is difficult because the entire solid-rotation zone would become solid for any Bn due to its lack of strain. Of course, the flow lines near the stationary point are not truly circular. By considering the problem of a rotating perturbed cylinder of radius $R(\theta) = 1 + \epsilon \sin \theta$, $\epsilon \ll 1$, we may be able to obtain a perturbed strain field that would show the dependence of the growth rate on Bn . We were unable to complete the analysis before the end of the workshop.

In this flow, there are actually an infinite number of eddies which approach the corner as an accumulation point (Leal, 1992, p. 158). Therefore, the corner will be stress-free as well and a dead zone may form there.

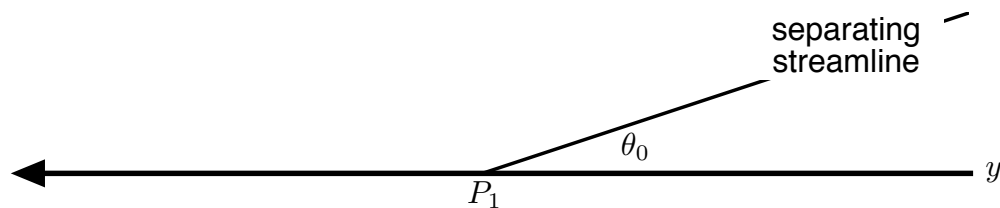


Figure 4.5. Flow near P_1 . The figure for P_2 is the mirror image, with x replacing y .

We next consider the flow near the stagnation points P_1 and P_2 where the separating streamlines connect to the wall (see Figure 4.5). From Batchelor (1967), p. 226,

$$\psi = Ar^3 \sin^2 \theta \sin(\theta_0 - \theta), \quad (4.8)$$

where θ_0 is the angle at which the streamline hits the wall. (It can be shown that (4.8) is a special case of (4.2) with $\lambda = 3$.) Since $\psi = O(r^3)$, the velocities are $O(r^2)$ and $T = O(r)$ as $r \rightarrow 0$. Therefore, this is also a region which should become plastic when $\text{Bn} \neq 0$. In

particular, the Bingham term (3.3a) will come into play when $|T| > \text{Bn}$, so the radius of the dead zone must grow like Bn .

Thus we expect that as $\text{Bn} \rightarrow 0$, but $\text{Bn} \neq 0$, there will be small plastic zones about the stagnation points and the eddy centers. They are different in that we expect the plastic zones about the stagnation points to be dead zones where the plastic is stationary, while the zones about the eddy centers may revolve in solid body rotation. As Bn increases, the sizes of the dead zones increases, and the speed of the rotation of the eddy zones slows. Eventually they will merge in a quick transition, and the entire region under the separating streamline becomes a dead zone. This reasoning is consistent with the simulations in Jay *et al.*, 2002.

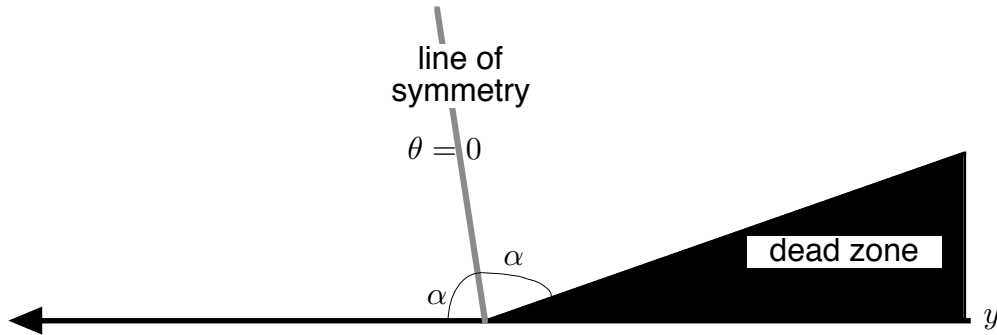


Figure 4.6. Stream function localization near dead zone.

We next wish to examine the angle of intersection of the dead zone with the wall. The dead zone forms a new rigid surface that behaves like another wall, so we may use our corner analysis of before, as shown in Figure 4.6. In particular, from (4.2) and (4.7) we see that the stresses are $O(r^{\lambda-2})$. Therefore, if $\lambda > 2$, there would be no strain, and hence from the Bingham law we would expect the dead zone to continue to grow. Therefore, at steady state we expect $\lambda \leq 2$.

Rewriting (4.5a), we obtain

$$\frac{\sin(2\alpha)}{2\alpha} = -\frac{\sin(2(\lambda-1)\alpha)}{2(\lambda-1)\alpha}. \quad (4.9)$$

Therefore, to obtain λ for any α , we simply compute $A = \sin(2\alpha)/2\alpha$ for that value of α , and then find the value of $\alpha_* = (\lambda-1)\alpha$ for which the right-hand side equals $-A$. This process is illustrated in Figure 4.7, where we see that for $\alpha = 1.43$, $A = 0.1$. Then for the same function to equal -0.1 , $\alpha_* = 1.75 > \alpha$, so $\lambda > 2$. However, we see from the graph that $\alpha_* > \alpha$ for all $\alpha < \pi/2$.

But we know that there is a finite strain against a flat wall, which corresponds to $\lambda = 2$. This can be verified by taking the limit that $\lambda \rightarrow 2$ in (4.2), which results in

$$\psi = r^2(A_c \cos 2\theta + B_s), \quad (4.10)$$

where we have used our symmetry condition. Since this is a regular limit, we may take the same limit in (4.5a), which yields

$$\sin(2\alpha) = -\sin(2\alpha),$$

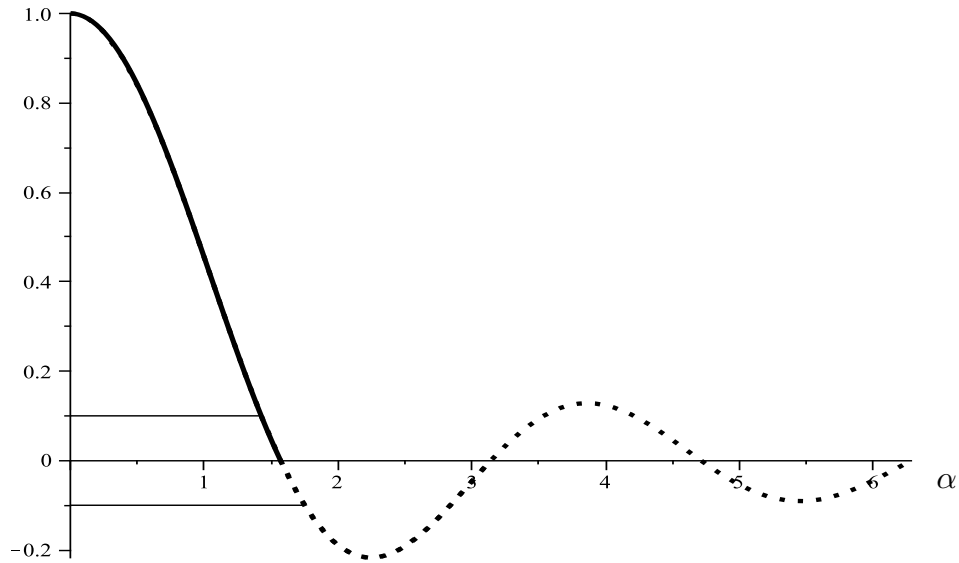


Figure 4.7. Plot of $(\sin 2\alpha)/2\alpha$ vs. α (general solution procedure). Solid line corresponds to angles of interest.

which implies that $\alpha = \pi/2$, the expression for a flat wall. Hence we see that the dead zone must approach the wall quadratically in x . Since Figure 4.6 may also be flipped horizontally, we see that we arrive at the same conclusion for the behavior of the dead zone near the floor.

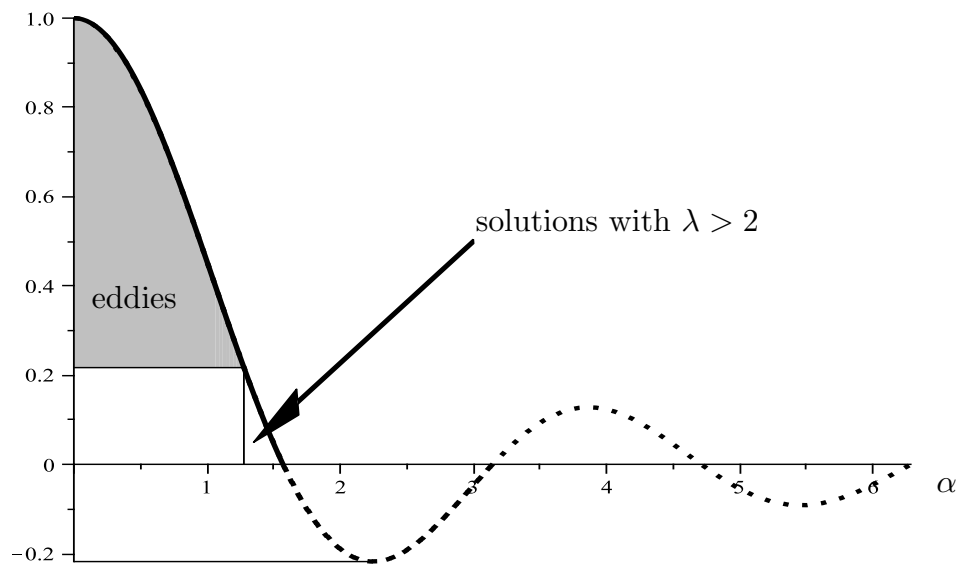


Figure 4.8. Plot of $(\sin 2\alpha)/2\alpha$ vs. α (limiting value). Solid line corresponds to angles of interest.

This analysis also indicates how we may eliminate dead zones. The dead zones form because of eddies in the Stokes flow. These eddies occur when (4.9) does not have a real

solution, which as shown in Figure 4.8, occurs when α is less than a minimum value, which can be computed as (Acheson, 1990, p. 232)

$$2\alpha_* \approx 146.3^\circ.$$

Therefore, creating a tank with a sloped edge with α greater than that value should eliminate eddies and perhaps dead zones.

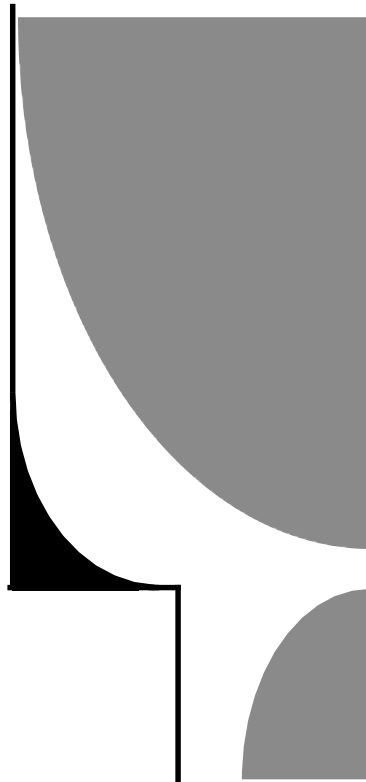


Figure 4.7. Tank flow for high Bingham number. The shaded regions are where the fluid is plastic, but moving. The dead zone is in black.

Though the analysis above shows how dead zones form, in our system the Bingham number is quite large (see Appendix). In this case, we see from (3.3) that unless the stress is extremely high, the strain rate will be zero and the fluid will behave as a plastic. Thus upstream there will be a small liquefied region near the walls where the stress is high, and the rest of the flow will be plastic plug flow (see Figure 4.7).

This liquefied region will widen as you move toward the wall (though not to the extent shown in Figure 4.7, which is not shown to scale). In the Lagrangian frame, fluid near the centerline moves in plastic flow until it experiences enough stress that it liquefies, and then continues to flow downward. The presence of the corners cause enough stress for the entire fluid to liquefy near $y = 0$, but then as the flow moves down the extrusion channel, the stress decreases and the flow becomes plastic again.

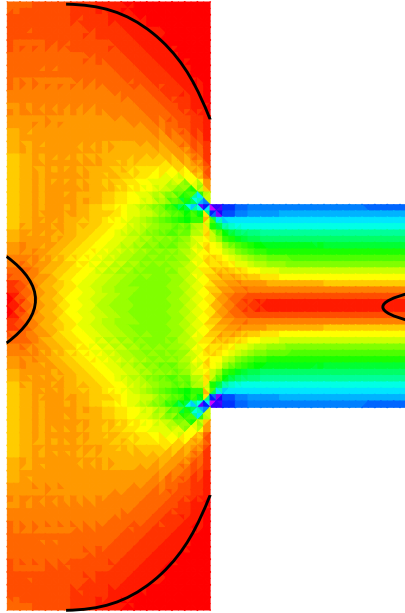


Figure 4.8. Strain for Stokes flow through a constriction.

Note that in contrast to the dead zones, the plastic regions in the core would not be seen after the extrusion process had ended, since that fluid would have been extruded.

The diagram in Figure 4.7 is consistent with the simulated strain diagram for Stokes flow, which is shown in Figure 4.8. Note the black contours surrounding areas of low strain, which would then correspond to the plastic plugs and dead zones.

Section 5: A Model Free-Boundary Problem

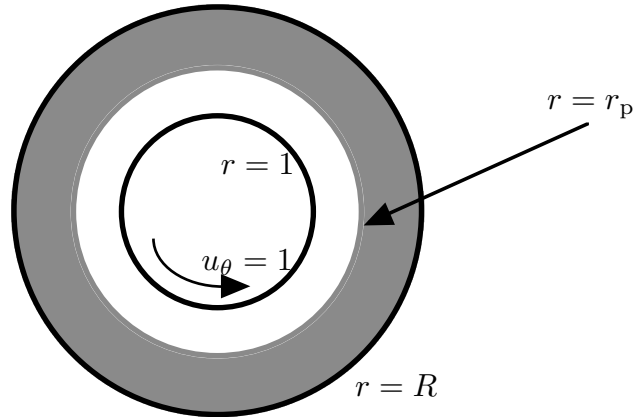


Figure 5.1. Couette flow of a Bingham fluid. The shaded regions are where the fluid is plastic, but moving.

In order to better understand what happens when the rotating plastic region nears the dead zone or wall, we wish to examine a simpler model problem. Consider normalized Couette flow of a Bingham fluid in the region $1 \leq r \leq R$ between two cylinders, as shown in Figure 5.1. Here the outer cylinder is held fixed. In particular, we have that the boundary conditions are

$$u_r(1, \theta) = u_r(R, \theta) = u_\theta(R, \theta) = 0, \quad u_\theta(1, \theta) = 1. \quad (5.1)$$

Hence we note that $u_r = 0$ and u_θ will be a decreasing function of r only. Hence from (4.7) the only stress term that survives is the shear stress

$$r \frac{d}{dr} \left(\frac{u_\theta}{r} \right). \quad (5.2)$$

But in this unidirectional shear flow, we see from the polar analog of (3.5) that

$$|E| = \left| r \frac{d}{dr} \left(\frac{u_\theta}{r} \right) \right| = \pm E, \quad (5.3)$$

depending on the sign of E . To determine the sign, we solve the problem with $\text{Bn} = 0$. Motivated by equation (7-15) in Leal (1992), we note that the variance of the pressure in the θ -direction is small, so we have, using Bird *et al.* (1960), p. 85 to get the momentum balance in the liquefied region:

$$\frac{1}{r^2} \frac{d}{dr} (r^2 \tau_{r\theta}) = 0$$

$$\tau_{r\theta}(r) = -\frac{2A}{r^2}, \quad (5.4a)$$

$$\begin{aligned} \frac{d}{dr} \left(\frac{u_\theta}{r} \right) &= -\frac{2A}{r^3} \\ \frac{u_\theta}{r} &= \frac{A}{r^2} + B \\ u_\theta(r) &= \frac{A}{r} + Br. \end{aligned} \quad (5.4b)$$

Substituting (5.4b) into the boundary conditions in (5.1), we obtain the following:

$$\begin{aligned} u_\theta(1) &= A + B = 1 \\ u_\theta(R) &= \frac{A}{R} + BR = 0 \end{aligned} \quad \implies \quad A = \frac{R^2}{R^2 - 1} > 0,$$

which ensures that $\tau_{r\theta} < 0$ from (5.4a).

Therefore, $|E| = -E$ in the Bingham case and (3.3) becomes

$$\tau_{r\theta} = r \frac{d}{dr} \left(\frac{u_\theta}{r} \right) - \text{Bn}, \quad \tau_{r\theta} < -\text{Bn}, \quad (5.5a)$$

$$\frac{d}{dr} \left(\frac{u_\theta}{r} \right) = 0, \quad \tau_{r\theta} > -\text{Bn}. \quad (5.5b)$$

Hence we have to substitute (5.5a) into (5.4a) in the liquefied region:

$$\begin{aligned} \frac{d}{dr} \left(\frac{u_\theta}{r} \right) - \frac{\text{Bn}}{r} &= -\frac{2A}{r^3} \\ \frac{u_\theta}{r} - \text{Bn} \log r &= \frac{A}{r^2} + B \\ u_\theta(r) &= \frac{A}{r} + Br + \text{Bnr} \log r. \end{aligned} \quad (5.6)$$

From (5.4a) we see that $|E|$ decreases as r increases. Hence the dead zone forms against the outer wall, which is the opposite of the physical situation in the previous section. This is because here an imposed force is causing the rigid body rotation in the center, while in the previous section the eddy is being rotated by the fluid which surrounds it, which may be slowing with increasing Bn. The participants are not aware of similar modeling of this example with which to check the results.

Therefore, (5.6) must hold for $1 \leq r \leq r_p$, where the subscript ‘‘p’’ stands for ‘‘plastic’’. At $r = r_p$, the following conditions hold:

$$u_\theta(r_p, \theta) = 0, \quad \tau_{r\theta}(r_p, \theta) = -\text{Bn}. \quad (5.7)$$

Substituting (5.6) and (5.4a) into (5.7) and the condition at $r = 1$, we have

$$\tau_{r\theta}(r_p) = -\frac{2A}{r_p^2} = -\text{Bn}$$

$$u_\theta(1) = A + B = 1$$

$$u_\theta(r) = \frac{\text{Bn}r_p^2}{2} \left(\frac{1}{r} - r \right) + r + \text{Bn}r \log r. \quad (5.8)$$

$$u_\theta(r_p) = \frac{\text{Bn}r_p^2}{2} \left(\frac{1}{r_p} - r_p \right) + r_p + \text{Bn}r_p \log r_p = 0$$

$$\text{Bn}r_p(1 - r_p^2 + 2 \log r_p) = -2r_p$$

$$\text{Bn} = \frac{2}{r_p^2 - 1 - \log r_p^2}. \quad (5.9)$$

A typical velocity profile is sketched in Figure 5.2. Note that the velocity is exactly zero for $r > r_p$.

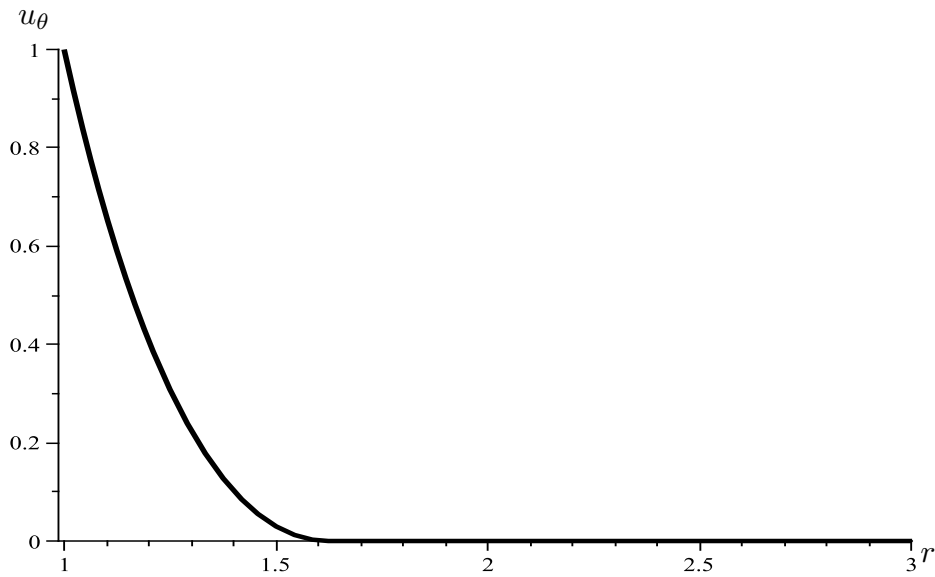


Figure 5.2. u_θ vs. r for $\text{Bn} = 3$ ($r_p = 1.62$) and $R = 3$.

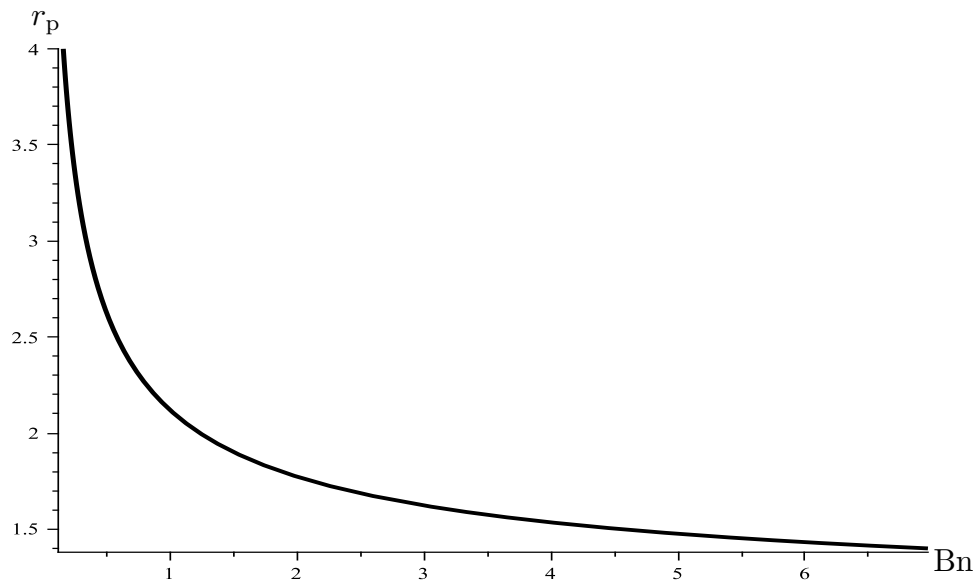
Equation (5.9), which is graphed in Figure 5.3, defines r_p implicitly in terms of Bn . Note that $r_p = R$ for some finite value of Bn , since as $\text{Bn} \rightarrow 0$,

$$\text{Bn} \sim \frac{2}{r_p^2}$$

$$r_p \sim \sqrt{\frac{2}{\text{Bn}}} \rightarrow \infty. \quad (5.10)$$

In other words, since there is always some finite shear stress at the outer wall, the effect of the Bingham flow will not be felt until Bn reaches some finite threshold. Also, as $\text{Bn} \rightarrow \infty$, we let $r_p^2 = 1 + r_1$, $r_1 \ll 1$, to obtain

$$\text{Bn} = \frac{2}{r_1 - \log(1 + r_1)} \sim \frac{2}{r_1 - (r_1 - r_1^2/2)} = \frac{4}{r_1^2} = \frac{4}{(r_p^2 - 1)^2}$$

Figure 5.3. r_p vs. Bn .

$$\begin{aligned}
 r_p^2 - 1 &\sim \frac{2}{\sqrt{Bn}} \\
 r_p &\sim \sqrt{1 + \frac{2}{\sqrt{Bn}}} \sim 1 + \frac{1}{\sqrt{Bn}}.
 \end{aligned}
 \tag{5.11}$$

Section 6: The Flow Cell

We next consider the flow cell, where the wall on the left is replaced by a line of symmetry. This is the only change, so the equations in section 2 hold with (2.7b) replaced by

$$\frac{\partial u_y}{\partial x}(0, y) = 0. \quad (6.1)$$

With this replacement, we no longer see eddies near the corner. In particular, since $u_x(x, 0) = u_x(0, y) = 0$, we must have that

$$u_x(x, y) \sim Axy, \quad (x, y) \rightarrow (0, 0), \quad (6.2a)$$

for some constant A . Therefore, by (2.8) we must have that

$$u_y(x, y) \sim -\frac{Ay^2}{2}, \quad (x, y) \rightarrow (0, 0), \quad (6.2b)$$

which satisfies (6.1). Due to the quadratic nature of these terms, we see that $T = O(x) = O(y)$ as these variables go to zero. Therefore, this is a region which should become plastic when $\text{Bn} \neq 0$. In particular, the Bingham term (3.3a) will come into play when $|T| > \text{Bn}$, so x , y , and hence the radius of the dead zone must grow like Bn .

We next wish to examine the angle of intersection of the dead zone with the boundaries. Near the floor, the geometry is exactly the same as in the tank case, so we expect the dead zone to attach tangent to the floor. However, near the line of symmetry, the analysis is different.

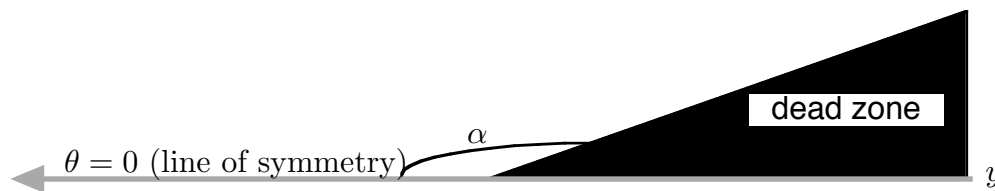


Figure 6.1. Stream function localization near dead zone.

We again try a solution of the form (4.2), but with the geometry as shown in Figure 6.1. Note that due to the symmetry of the problem, we may measure α in the clockwise direction without affecting our solution. Note also that this makes the region of interest $\alpha \in [\pi/2, \pi)$.

Hence we replace (4.4) with

$$\frac{\partial \psi}{\partial r}(r, \alpha) = \frac{\partial \psi}{\partial \theta}(r, \alpha) = 0. \quad (6.3)$$

Moreover, the problem is symmetric about $\theta = 0$ with

$$\begin{aligned} u_r(r, \theta) &= u_r(r, -\theta) \\ \frac{\partial \psi}{\partial \theta}(r, \theta) &= \frac{\partial \psi}{\partial \theta}(r, -\theta), \end{aligned} \quad (6.4)$$

which forces $A_c = B_c = 0$. Note that since the biharmonic equation is fourth order, we cannot use just the more standard boundary condition

$$\frac{\partial u_r}{\partial \theta}(r, 0) = 0,$$

since imposing this would result in an equation for A_c in terms of B_c .

We now wish to satisfy the conditions (6.3) at $\theta = \alpha$. Hence we have

$$\begin{aligned} \frac{\partial \psi}{\partial r}(r, \alpha) &= \lambda r^{\lambda-1} [A_s \sin(\lambda\alpha) + B_s \sin((\lambda-2)\alpha)] = 0 \\ \frac{\partial \psi}{\partial \theta}(r, \alpha) &= r^\lambda [A_s \lambda \cos(\lambda\alpha) + B_s (\lambda-2) \cos((\lambda-2)\alpha)] = 0 \\ &-\sin((\lambda-2)\alpha) \lambda \cos(\lambda\alpha) [\sin(\lambda\alpha)]^{-1} + (\lambda-2) \cos((\lambda-2)\alpha) = 0, \end{aligned}$$

where we have set the bracketed quantities in the first two equations equal to zero and set $B_s = 1$ without loss of generality. Continuing to simplify, we obtain

$$\begin{aligned} -(\lambda-1) \sin((\lambda-2)\alpha) \cos(\lambda\alpha) + (\lambda-1) \cos((\lambda-2)\alpha) \sin(\lambda\alpha) \\ = \sin((\lambda-2)\alpha) \cos(\lambda\alpha) + \cos((\lambda-2)\alpha) \sin(\lambda\alpha) \\ (\lambda-1) \sin(2\alpha) = \sin(2(\lambda-1)\alpha) \\ \frac{\sin(2\alpha)}{2\alpha} = \frac{\sin(2(\lambda-1)\alpha)}{2(\lambda-1)\alpha}. \end{aligned} \quad (6.5)$$

Note that (6.5) is of the form of (4.9), with the exception of a change of sign.

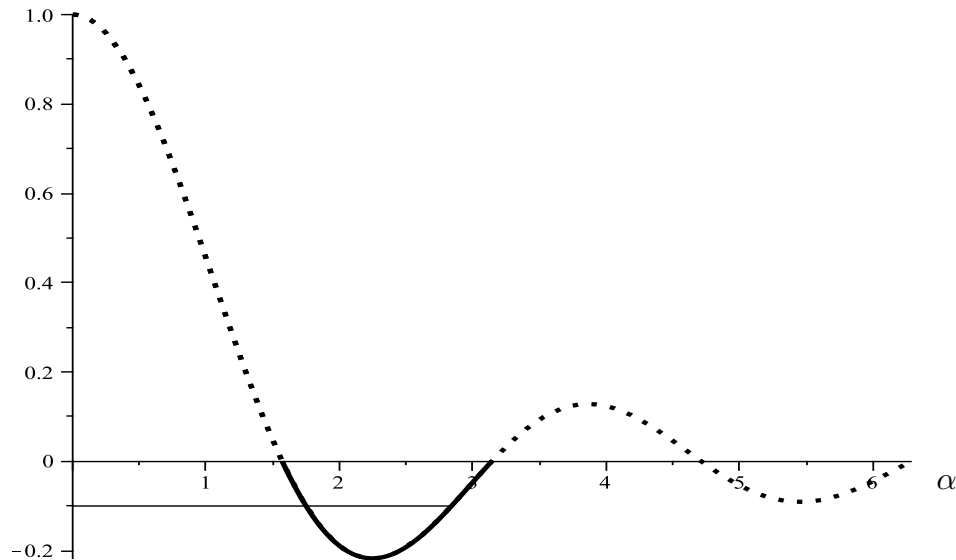


Figure 6.2. Plot of $(\sin 2\alpha)/2\alpha$ vs. α . Solid line corresponds to angles of interest.

Hence there is a change of procedure in finding λ in the region of interest. To obtain λ for any α , we simply compute $A = \sin(2\alpha)/2\alpha$ for that value of α , and then find the adjacent value of α (call it α_*) for which the function also equals A . This process is illustrated in Figure 6.2, where we see that for $\alpha = 1.75$, $A = -0.1$. The adjacent crossing is $\alpha_* = 2.8 > \alpha$, so $\lambda > 2$, which corresponds to zero stress at the origin. However, if we instead had started with $\alpha = 2.8$, then $\alpha_* = 1.75 < \alpha$, so $\lambda < 2$, which corresponds to infinite stress at the origin.

As shown from the graph, the transition between these two cases occurs at the first minimum of the function, which corresponds to $\alpha = 3\pi/4$. Therefore, we expect this angle to correspond to finite strain, especially since it matches experimental observations of peaks in the dead zones near the cell floor.

However, this is not so easy to establish theoretically, for several reasons:

1. Since $\alpha = 3\pi/4$ corresponds to the minimum of the function plotted in Figure 6.2, we see that there does not exist an α_* which will have the same value.
2. $\lambda = 2$ is a singular limit of (6.5), since this equation has a solution for all α with $\lambda = 2$.
3. $\lambda = 2$ is a singular limit of (4.2).

Referencing Leal (1992), equation (4-118), we see that the appropriate eigenfunction for $\lambda = 2$ subject to (6.4) is

$$\psi = r^2(A_s \sin 2\theta + B_s \theta). \quad (6.6)$$

(Note there is a typographical error in Leal (1992), equation (4-119).)

We now wish to satisfy the conditions at $\theta = \alpha$. Hence we have

$$\begin{aligned} \frac{\partial \psi}{\partial r}(r, \alpha) &= 2r [A_s \sin(2\alpha) + B_s \alpha] = 0 \\ \frac{\partial \psi}{\partial \theta}(r, \alpha) &= r^2 [2A_s \cos(2\alpha) + B_s] = 0 \\ \sin(2\alpha) - 2\alpha \cos(2\alpha) &= 0, \end{aligned}$$

where we have set the bracketed quantities in the first two equations equal to zero and set $A_s = 1$ without loss of generality. Continuing to simplify, we obtain

$$\tan 2\alpha = 2\alpha. \quad (6.7)$$

The first root of this equation is at $\alpha = 2.25$. But this value is less than $3\pi/4$, and hence is in the region where the first λ from (4.2) is greater than 2. Therefore, it might be this value at which the dead zone forms.

Now consider the case of high Bn. Because of this replacement, the slurry flows in plastic plug flow for large y , and there is no liquid shear layer near $x = 0$. As the fluid flows toward the floor, normal stresses begin to liquefy the fluid. In the region away from $x = 0$, the behavior near the outlet is similar for both the tank and cell flows.



Figure 6.3. Cell flow for high Bingham number. The shaded regions are where the fluid is plastic, but moving. The dead zone is in black.

Section 7: Fluids with a Yield Stress in a Thin Geometry

In this section we explore flow in a thin geometry either with a free surface, or in a channel or pipe with slowly varying walls. The original intent was that perhaps the thin geometry could be used to get a simpler problem to see a dead zone near a contraction; we shall see that this will not happen with any of the approaches for thin flows that we located.

The challenge of using a Bingham or Hershel-Bulkley fluid in a thin geometry is that one can obtain a contradiction in trying to solve for the moving plug where the stresses are low. One would like to get a plug that is unyielded (as is required by the models), but unless one does the expansions for lubrication theory carefully, one will get a plug that is non-uniform due to extensional flow. The secret seems to be to keep the variations mild enough to be able to correct them at the next order so that the plug can be made uniform.

The consistent lubrication theory was first developed by Balmforth and Craster (1999) and was used to model lava flow down an inclined plane. (See also Griffiths (2000), Balmforth *et al.* (2002), *e.g.*, and the confined channel flow of Wei and Yuhi (2001).) In Balmforth and Craster (1999), they develop a consistent perturbation approach to get a uniform plug flow with a two-layer film consisting of a plug overlying a Poiseuille flow above a flat plate; the flow is driven down the inclined plane due to the pressure gradient caused by gravity. The analysis allows one to do a consistent procedure without resorting to a biviscous model.

Closer to the problem of interest in the workshop is the paper by Frigaard and Ryan (2004) which studies the flow in a thin channel with slowly varying walls that are symmetric about the mid-plane and that has the flow driven by a pressure gradient. We now describe some of the salient aspects of that work.

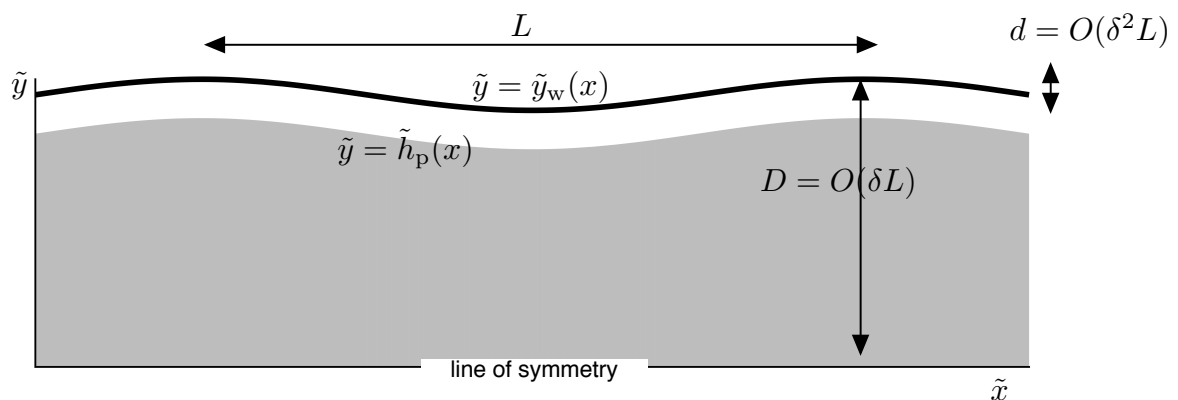


Figure 7.1. Schematic of flow in Frigaard and Ryan (2004).

The flow in Frigaard and Ryan (2004) is bounded by walls with the periodic function $\tilde{y} = \pm\tilde{y}_w(x)$; we will concentrate on the upper side with the plus sign (see Figure 7.1).

Here x is the streamwise coordinate and y is the cross-stream coordinate. The average half width is D , and the period of \tilde{y}_w is L ; the ratio $\delta = D/L \ll 1$ is the small parameter. The specific function used in Frigaard and Ryan (2004) was $\tilde{y}_w = D + d \cos(2\pi x)$, with $h = O(\delta D)$; this small size of the oscillation in the wall, that is, $d = O(\delta^2 L)$, is crucial for the consistent perturbation method to work. A major objective is to solve for the location of the plug boundary; to leading order, a plug in the interval $|y| \leq h_p(x)$ is found but has a speed that depends on x , and so it will be called a pseudoplug in this case.

Now scaling in a way similar to the standard lubrication approach (*i.e.*, as was done in Frigaard and Ryan (2004)), then one can solve the leading order problem for the axial (streamwise) velocity u_x :

$$u_x(x, y) = \frac{B}{2h_p}(y_w - h_p)^2 \left[1 - \frac{(y - h_p)^2}{(y_w - h_p)^2} \right], \quad y \in [h_p, y_w], \quad (7.1a)$$

$$u_x(x, y) = \frac{B}{2h_p}(y_w - h_p)^2, \quad y \in [0, h_p]. \quad (7.1b)$$

Equation (7.1a) describes the Poiseuille flow near the wall, while (7.1b) describes the pseudoplug flow in the interior. It is called a pseudo-plug flow because the plug still has x dependence because of extensional flow. There is no shear on the plug but even though it is supposed to be unyielded and moving with constant speed, it is in fact deforming.

If $d = O(\delta D)$ in \tilde{y}_w , then one can show that the leading order expression simplifies to

$$u_x \approx \frac{Bh_p}{2} \left(\frac{1}{h_p} - 1 \right)^2 + O(\delta).$$

This expression implies that the x -dependence from the wall is postponed to higher order, and the leading order location for the boundary of the pseudoplug h_p may now be made constant. These two combine to give us a consistent leading order plug flow behavior, but the spatial variation from extensional flow has simply been pushed off to the next order. The consistent perturbation approach can determine, using matching or patching, corrections to $u(x)$ that eliminate the x -dependence for sufficiently mild wall variation which maintaining unyielded plug flow and it generates corrections to the location of the boundary of the plug. The corrected plug boundary is referred to as the true yield surface $y_T(x)$.

The paper Frigaard and Ryan (2004) can also estimate when the plug will break as the variation in the wall variation amplitude h increases. The critical amplitude d_c is still proportional to $\delta^2 L$ based on estimating the average stress across the plug, and using the consistent theory as a basis for the estimate. Thus, this theory suggests that mild contractions in the channel width cause a plug to break (as seen in numerical simulations in the literature), but it will not be able to capture dead zones near a wall with the slowly varying limitation.

This consistent procedure avoids the use of biviscous models for the fluid that have been developed by Wilson (cf. Wilson, 1999). In Balmforth and Craster (1999) and Frigaard and Ryan (2004), there is some concern about the limit taken when using the biviscous model. We also note that the developing flow in a channel was also treated by Wilson and coworkers (Wilson and Taylor, 1996; Khatib and Wilson, 2001).

Section 8: Conclusions and Further Research

A key fact that the previous analysis missed is that the dead zone is not only stationary—it is also dry. In much the same way that a sponge under pressure will extrude water, the high pressure near the wall is extruding water from the slurry in that region. The slurry is really a mix of solid and liquid. Near the wall, the water can move much more easily than the solid, so it does, drying out the dead zone.

An accurate treatment of this phenomena would involve modeling the slurry as a two-phase flow. Hence the equations of section 3 would have to be coupled to transport equations in the solid.

Appendix

For the individual flow cell, the parameters are as follows:

$$L_i = 3 \text{ mm}, \quad L_o = 0.3 \text{ mm}. \quad (\text{A.1})$$

These values were taken from a typical extrusion product brought to the workshop. The exact depth of the extrusion chamber was unknown, but it seems to be on the order of an inch or so. Therefore, to keep the ratio of 10:1 from (A.1), we chose

$$H = 3 \text{ cm}. \quad (\text{A.2})$$

The product is extruded at a rate of roughly 1 inch/s, which we adapt to 3 cm/s. Assuming the velocity is constant across input and output and keeping the flow rate constant, we have

$$u_c = \frac{L_o}{L_i} \left(3 \frac{\text{cm}}{\text{s}} \right) = 3 \frac{\text{mm}}{\text{s}}. \quad (\text{A.3})$$

We did not discuss any particular parameters for the tank, except for the fact that it has a contraction ratio of about 1:2 and H can still be taken large enough such that the flow is well-developed in the region of interest.

For the material properties, we use the following:

$$\tau_c = 2 \times 10^5 \text{ Pa}, \quad \eta_c = 250 \text{ Pa} \cdot \text{s} \quad \implies \quad \text{Bn} = \frac{(2 \times 10^5 \text{ Pa})(3 \text{ mm})}{(3 \text{ mm/s})(250 \text{ Pa} \cdot \text{s})} = 800.$$

where the yield stress was given by the presenter and the viscosity value (chosen to get an order-of-magnitude estimate) is for peanut butter from Wikipedia (2009).

For the density ρ , we use the following value for wet lump clay from SIMetric (2009):

$$\rho = 1602 \frac{\text{kg}}{\text{m}^3}, \quad (\text{A.4})$$

which makes the Reynolds number in the flow cell

$$\text{Re} = \left(1602 \frac{\text{kg}}{\text{m}^3} \right) \frac{3 \text{ mm}}{250 \text{ kg/m} \cdot \text{s}} \left(3 \frac{\text{mm}}{\text{s}} \right) = (9 \times 10^{-6} \text{ m}^2) \left(\frac{6.4}{\text{m}^2} \right) = 5.77 \times 10^{-5}. \quad (\text{A.5})$$

Nomenclature

Units are listed in terms of length (L), mass (M), or time (T). If the same letter appears both with and without tildes, the letter with a tilde has dimensions, while the letter without a tilde is dimensionless. The equation number where a particular quantity first appears is listed, if appropriate.

- A : arbitrary constant, variously defined.
- B : arbitrary constant, variously defined.
- Bn: Bingham number (3.3a).
- d : oscillation amplitude in Frigaard-Ryan model, L .
- D : height parameter in Frigaard-Ryan model, L .
- $\tilde{E}(\tilde{x}, \tilde{y})$: strain tensor, T^{-1} (2.11).
- H : height of tank, L .
- $\tilde{h}(\tilde{x})$: free boundary, L .
- L : length scale in \tilde{x} -direction, L .
- ℓ : dimensionless ratio L_o/L_i (2.6).
- P : point where separating streamline attaches to wall.
- $\tilde{p}(\tilde{x}, \tilde{y})$: pressure, M/LT^2 (2.10a).
- $\tilde{T}(\tilde{x}, \tilde{y})$: stress tensor, M/LT^2 .
- R : outer radius in Couette flow problem (5.1).
- r : local polar coordinate (4.1).
- Re: Reynolds number (2.9).
- $\tilde{u}(\tilde{x}, \tilde{y})$: velocity, L/T .
- \tilde{x} : distance along tank floor, L .
- \tilde{y} : height above tank floor, L .
- α : wall angle.
- β : parameter in exponential model (3.7), T .
- δ : small parameter.
- η : viscosity, M/LT (2.9).
- θ : local angular coordinate (4.1).
- λ : exponent in stream function (4.2).
- ρ : density, M/L^3 (2.9).
- $\tilde{\tau}(\tilde{x}, \tilde{y})$: component of the stress tensor \tilde{T} , M/LT^2 (2.10a).
- ψ : stream function (4.1).

Other Notation

- c: as a subscript, used to indicate a characteristic value (2.3) or cosine (4.2).

- d: as a subscript, used to indicate the dead zone.
- i: as a subscript, used to indicate input.
- o: as a subscript, used to indicate output.
- p: as a subscript, used to indicate the Bingham free boundary (5.7).
- r : as a subscript, used to indicate the radial direction (4.1).
- s: as a subscript, used to indicate sine (4.2).
- w: as a subscript, used to indicate the wall.
- x : as a subscript, used to indicate the x -direction.
- y : as a subscript, used to indicate the y -direction.
- θ : as a subscript, used to indicate the angular direction (4.1).

References

- Abdali, S. S., Mitsoulis, Evan, and Markatos, N. C. “Entry and exit flows of Bingham fluids.” *J. Rheol.* **36** (1992): 389–407.
- Acheson, D. J. *Elementary Fluid Dynamics*. Oxford: Clarendon Press, 1990.
- Al Khatib, M. A. M., and Wilson, S. D. R. “The development of Poiseuille flow of a yield-stress fluid,” *J. Non-Newtonian Fluid Mech.* **100** (2001): 1–8.
- Balmforth, N., and Craster, R. V. “A consistent thin-layer theory for Bingham Plastics,” *J. Non-Newtonian Fluid Mech.* **84** (1999): 65–81.
- Balmforth, N. J., Craster, R. V., and Sassi, R. “Shallow viscoplastic flow on an inclined plane,” **47** (2002): 1–29.
- Batchelor, G. K. *An Introduction to Fluid Dynamics*. Cambridge: Cambridge University Press, 1967.
- Bird, R. B., Stewart, W. E., and Lightfoot, E. N. *Transport Phenomena*. New York: John Wiley and Sons, 1960.
- Frigaard, I. A., and Ryan, D. P. “Flow of a visco-plastic fluid in a channel of slowly varying width,” *J. Non-Newtonian Fluid Mech.* **12** (2004): 67–83.
- Griffiths, R. W. “The dynamics of lava flows,” *Annu. Rev. Fluid Mech.* **32** (2000): 477–518.
- Jay, P., Magnin, A., and Piau, J. M. “Numerical simulation of viscoplastic fluid flows through an axisymmetric contraction.” *Transact. AME* **124** (2002): 700–705.
- Leal, L. G.. *Laminar Flow and Convective Processes: Scaling Principles and Asymptotic Analysis*. Boston: Butterworth-Heinemann, 1992.
- Mei, C. C., and Yuhi, M. “Slow flow of a Bingham fluid in a shallow channel of finite width,” *J. Fluid Mech.* **431** (2001): 135–159.
- Moffatt, H. K. “Viscous and resistive eddies near a sharp corner.” *J. Fluid Mech.* **18** (1964): 1–18.
- Papanastasiou, T. C. “Flows of materials with yield.” *J. Rheol.* **31** (1987): 385–401.
- SIMetric, “Density of bulk materials.” http://www.simetric.co.uk/si_materials.htm. Accessed June 16, 2009.
- Smyrniotis, D. N., and Tsampoulos, J. A. “Squeeze flow of Bingham plastics.” *J. Non-Newtonian Fluid Mech.* **100** (2001): 165–190.
- Wikipedia, “Viscosity.” <http://en.wikipedia.org/wiki/Viscosity>. Accessed June 23, 2009.
- Wilson, S. D. R. “A note on thin-layer theory for Bingham plastics,” *J. Non-Newtonian Fluid Mech.* **85** (1999): 29–33.
- Wilson, S. D. R., and Taylor, A. J. “The channel entry problem for a yield stress fluid,” *J. Non-Newtonian Fluid Mech.* **65** (1996): 165–176.